Chemical Science

ROYAL SOCIETY OF CHEMISTRY

EDGE ARTICLE

View Article Online
View Journal | View Issue

Cite this: *Chem. Sci.*, 2025, **16**, 7227

All publication charges for this article have been paid for by the Royal Society of Chemistry

A bioimmune mechanism-inspired targeted elimination mechanism on the anode interface for zinc–iodine batteries†

Kaixin Wang,[a] Yuting He,[a] Ruduan Yuan,[a] Zhaoyu Chen,[a] Qianzhi Gou,[ab] Sida Zhang,[a] Huaping Mei,[b] Yujie Zheng,[a] John Wang[cd] and Meng Li*[a]

Alkaline byproducts at the zinc anode interface continue to exacerbate subsequent side reactions, so realizing timely salvage of electrodes is equally important compared to upfront prevention strategies. Although the utilization of acid electrolytes could eliminate by-products on the Zn anode, they inevitably exacerbate the undesired hydrogen evolution reaction. Therefore, achieving elimination of by-products without exacerbating other side reactions is urgently needed. Inspired by the immune protection mechanisms in organisms, facile cysteamine hydrochloride (Cy-H) additives were incorporated into the aqueous electrolyte to stabilize the anode. Concretely, the Cy-H additives can reconstruct the electrical double layer (EDL) on the Zn anode and inhibit drastic parasitic reactions and cooperate with electric fields and acidic environments, thus achieving the desired effect of targeted elimination of alkaline by-products. Ultimately, with a long calendar lifespan of 2000 h with a Zn anode carrying by-products and outstanding performance over 8000 cycles for the Zn||I_2 full cell, the assembled pouch battery also achieved 1000 cycles without capacity degradation. To further promote the practical applications, the inhibition mechanism of Cy-H additives on full-cell self-discharge was revealed. This work provides new insights for the use of strong acid electrolytes and the elimination of interfacial by-products in aqueous zinc–iodine batteries.

Received 3rd January 2025
Accepted 21st March 2025

DOI: 10.1039/d5sc00040h

rsc.li/chemical-science

Introduction

Among the existing energy storage systems, the zinc–iodine battery realizes the storage and release of electric energy through the redox reaction of the cathode in conjunction with the deposition/stripping of the Zn anode, which has considerable feasibility and economic benefits.[1] However, in the process of Zn^{2+} deposition/stripping, the HER inevitably occurs due to the intrinsic characteristics of the aqueous electrolyte, releasing OH^-, and Zn^{2+} will spontaneously form alkaline by-products [$Zn_4(OH)_6SO_4 \cdot xH_2O$] by reacting with OH^- and SO_4^{2-}.[2] The presence of by-products accelerates the generation and growth of Zn dendrites by changing the electric field distribution and reaction site distribution on the Zn anode interface, and ultimately,[3] the point discharge effect of Zn dendrites will cause an intense HER, forming a death cycle that continuously exacerbates the failure of the Zn anode (Fig. 1a).

Timely control of side reactions that have already occurred is equally important compared to the suppression of side reactions.[4] Otherwise, previous efforts to inhibit side effects may be in vain,[5] but this aspect is often neglected.[6] Among the three types of representative destructive behaviors,[7] the H_2 generated by the HER is difficult to reversibly return as a proton in solution, and the Zn dendrites that have been generated are also difficult to selectively remove due to their nature being the same as that of Zn electrodes,[8] and the only by-products that can be reversibly removed have become a breakthrough in the process of solving the deterioration of the Zn anode.[9] There is an urgent need for an effective by-product elimination strategy to break the death cycle at the Zn anode interface,[10] to effectively intervene in areas where by-products have already occurred.[11]

In previous by-product elimination strategies, Yu *et al.* avoided the accumulation of $Zn_4(OH)_6SO_4 \cdot xH_2O$ by catalyzing the production of NH_3 on the surface of the by-products and forming soluble complexes $[Zn(NH_3)_4]^{2+}$ with it with the help of urea molecules introduced into the electrolyte as a reactivator.[12] Qian *et al.* also regenerated dead Zn to electroactive Zn^{2+} by the

[a]National Innovation Center for Industry-Education Integration of Energy Storage, MOE Key Laboratory of Low-grade Energy Utilization Technologies and Systems, CQU-NUS Renewable Energy Materials & Devices Joint Laboratory, College of Energy & Power Engineering, Chongqing University, Chongqing 400044, China. E-mail: limeng@cqu.edu.cn

[b]School of Building Services Science and Engineering, Xi'an University of Architecture and Technology, Xi'an, 710055, China

[c]National University of Singapore (Chongqing) Research Institute, Chongqing 401123, China

[d]Department of Materials Science and Engineering, National University of Singapore, 117573, Singapore

† Electronic supplementary information (ESI) available. See DOI: https://doi.org/10.1039/d5sc00040h

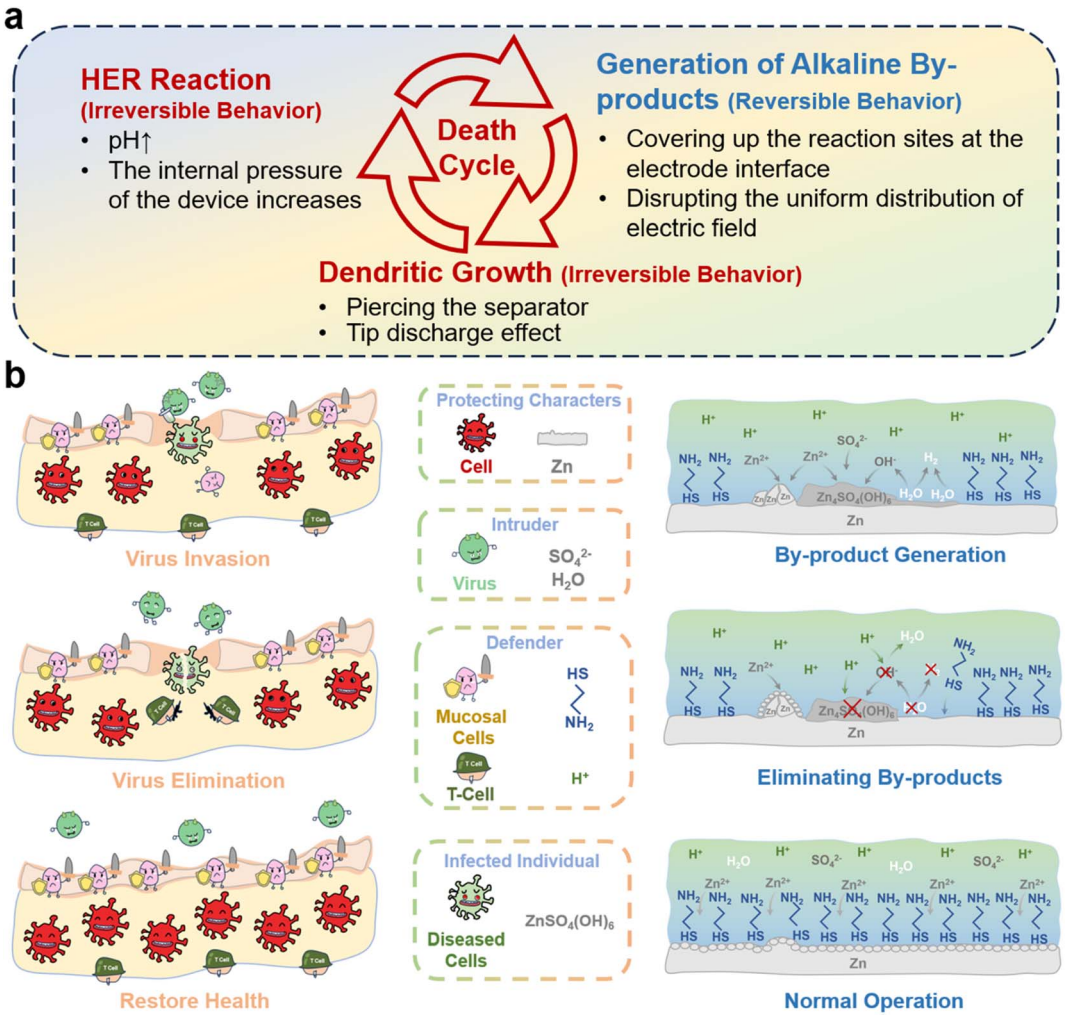

Fig. 1 (a) Schematic diagram of the death cycle of the Zn anode; (b) the working mechanism of the specific immune system of organisms and the specific elimination of by-products of Cy-H additives on the surface of the Zn anode.

introduction of ferrocene,[13] which effectively suppressed Zn corrosion and the formation of insulation by-products from dissolved oxygen. With limited additive concentrations,[14] water still occupies the majority of the coordination environment for Zn^{2+}, and thus achieving solubilization of by-products by ligand introduction is not an optimal strategy.[15] Using acid–base neutralisation reactions to eliminate by-products is a straightforward and effective strategy; however, the HER from acidic environments is unavoidable.[16] Therefore, Nian *et al.* introduced bisimide into the electrolyte, which formed a ZnS protective layer on the surface of the zinc negative electrode to resist the self-corrosion behavior while avoiding the accumulation of alkaline by-products on the surface,[17] effectively avoiding the occurrence of successive side reactions. However, the formation of ZnS consumes additional chemical and electrical energy and does not guarantee the homogeneity of the protective layer.[18] As a result, developing a strategy to eliminate by-products on the Zn anode without damaging the electrodes and consuming excessive electrical energy has the potential to increase the use of aqueous batteries for large-scale energy storage.[19]

The human body is frequently attacked by a variety of diseases, most of which are caused by viral infections.[20] Although the body's protective non-specific immune barrier blocks most viruses from invading the body, some viruses are still able to reach the body and infect healthy cells.[21] In this case, the body's specific immune mechanism sends T-cells to target and eliminate the infected cells without harming healthy cells (Fig. 1b).[22] Herein, inspired by the immune system in living organisms, an electrolyte additive that ensures the targeted elimination of by-products without causing additional corrosion and damage to the Zn anode is developed. Benefiting from the adsorption of Cy-H, the EDL structure on the Zn anode is modified, inhibiting the HER and regulating Zn deposition. The acidic environment brought about by Cy-H and the assistance of the electric field can eliminate the by-products in time, and the self-discharge behavior caused by the spontaneous diffusion of I_3^- is suppressed. With these advantages, the Zn symmetric cell using the Cy-H electrolyte additive can achieve 3000 h of stable cycling, and an amazing 2000 h of cycling was achieved with the use of a Zn electrode carrying lots of by-products, and the assembled Zn||I_2 full cell demonstrated 8000 cycles and 95%

capacity retention, and the assembled pouch battery also achieved 1000 cycles without capacity degradation. Finally, the full cell exhibited a low self-discharge rate of 97.45%. These results break the dilemma of zinc–iodine batteries that are difficult to cycle in acidic environments and provide a new reference and inspiration for the development of acidic electrolyte additives and by-product elimination strategies.

Results and discussion

In this work, the structure of the selected additive is shown in Fig. S1† and consists of a cysteamine salt molecule together with a hydrochloric acid molecule. Spectroscopic analysis was carried out to analyze the effect that this additive would have after being dissolved in the $ZnSO_4$ (ZSO) electrolyte.[23] The results are shown in Fig. 2a, where the ^1H peak in the nuclear magnetic resonance (NMR) of D_2O shifted from the original 4.71 ppm to a downfield of 4.65 ppm after adding 0.01 M Cy-H. It is possible that the additive hydrolyzed out the HCl molecules, affecting the potential of hydrogen (ph) of the electrolyte, which was analyzed according to the structural formula.[24] Therefore, 0.01 M HCl was added into 2 M ZSO for NMR testing and the results showed the same chemical shifts. This suggests that the addition of Cy-H may dissociate both Cy and HCl. Meanwhile, the ph test results of the electrolyte (Fig. 2b) also confirmed our inference that the addition of 0.01 M of Cy-H and HCl led to similar ph values of 2.3 and 2.2, respectively, while ZSO resulted in a value of 4.8.[25] In other words, the introduction of the additives turned the electrolyte into a strongly acidic liquid, which may not be favorable for use in zinc ion batteries.[26] To investigate the impact of ph on the cycling stability of the electrodes, the HER strength of electrolytes with varying ph levels was assessed using differential electrochemical mass spectrometry (DEMS).[27] The results, shown in Fig. 2c, indicate that the HER intensity increases progressively as the ph decreases. Specifically, at a ph of 5, the HER intensity is approximately 3.2×10^{12} (for a 2 M ZSO electrolyte). In contrast, the HER intensity of the Cy-H electrolyte, which has a ph of around 2, is approximately 1.7×10^{-10} A, nearly 100 times higher than that of ZSO.[28] This substantial difference in HER strength underscores the challenges associated with utilizing highly acidic proton-rich electrolytes, which can significantly impact the performance and stability of aqueous batteries.[29] Next, we targeted the cysteamine salt (Cy) isolated from the electrolyte. The binding energy of Cy to the Zn anode was calculated using density functional theory (DFT) (Fig. 2d). The lower adsorption energy (−0.924 eV) at the –SH of Cy reflects its spontaneous adsorption behavior on the Zn anode relative to the adsorption behavior at $–NH_2$ (−0.874 eV).[30] Meanwhile, MD simulations were performed to test the distribution of Cy-H in solution (Fig. 2e).[31] After the addition of Cy-H, the additive (Fig. 2f) aggregated in large amounts at the

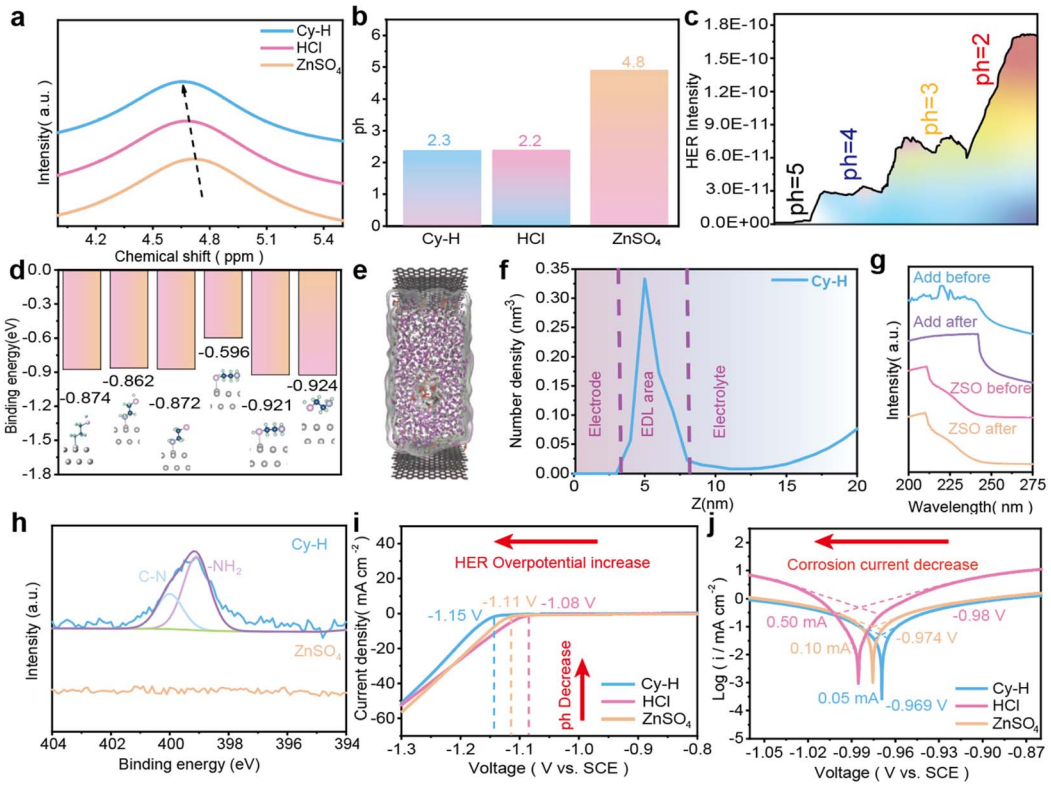

Fig. 2 The ^1H NMR (a) and ph (b) test results of various electrolytes; (c) the relationship between the HER intensity and electrolyte ph value; (d) adsorption energy of Zn (002) with different sites of Cy-H; (e) Cy-H obtained from MD simulations; (f) statistical results of the number density distribution of Cy-H in electrolyte; (g) UV-vis spectra of various electrolytes; (h) N 1s XPS spectra of the Zn anode after immersion; LSV curves (i) and Tafel plots (j) of the Zn anode in various electrolytes.

boundary of the IHP, with only a very small amount of distribution in the outer Helmholtz plane (OHP) as well as in the bulk phase, which proves the self-adsorption behavior of the additive at the interface.[32]

Subsequently, the same Zn anode was immersed in Cy-H and ZSO for 48 h. The ultraviolet-visible spectroscopy (UV-vis) spectral results of the electrolyte before and after immersion are shown in Fig. 2g, where before immersion the addition of Cy-H additives caused it to exhibit a different absorption peak shape than ZSO. The shape of the ZSO electrolyte did not change significantly after immersion, while the absorption peak of Cy-H fluctuated more significantly.[33] To exclude the fluctuation of the absorption peak caused by the change of ph, different dosages of HCl were added to ZSO, and the results are shown in Fig. S2,† which shows that the absorption peak shifted to the lower region with the decrease of ph, and it does not have any effect on the shape of the absorption peak.[34] Therefore, it can be concluded that the change in the absorption peak is due to spontaneous adsorption of Cy-H on the surface of the electrode, indicating that Cy can still spontaneously produce adsorption behavior on the surface of the Zn anode in an acidic environment.[35] The scanning electron microscope (SEM) images of the electrode after immersion are demonstrated in Fig. S3 and S4,† and the surface of the electrode immersed in ZSO showed a large number of particulate impurities, which may be the result of the serious byproduct formation of the Zn anode in the electrolyte, generating $Zn_4(OH)_6SO_4 \cdot xH_2O$, and the energy dispersive spectrometer (EDS) result (Fig. S5†) also shows that the constituent elements of the particles are mainly the elements O and S.[36] On the other hand, the surface of the Zn anode after immersion in Cy-H still maintained a smooth morphology, and no particle generation was observed, and the EDS results (Fig. S6†) showed that the main elements present on the surface of the dipped Zn anode were N and S, which also confirmed the adsorption behavior of Cy.[37] In order to eliminate the interference of HCl, the same Zn anode was immersed in HCl (0.01 M HCl + 2 M ZSO) for a duration of 48 h. The SEM results are displayed in Fig. S7.† The generation of by-products was not observed on the surface of the Zn anode; instead, there were massive craters, which may have been formed due to the strongly acidic environment resulting in significant chemical corrosion of the Zn anode.[38] This indicated that Cy-H could keep the Zn anode stable in the electrolyte, avoiding the production of by-products on its surface and also protect the electrode from corrosion in the acidic solution, which was amazing. It was further confirmed that the composition of the product was $Zn_4(OH)_6SO_4 \cdot xH_2O$.[39] In contrast, the Zn anode after Cy-H immersion showed only characteristic peaks of Zn, according to the X-ray diffraction (XRD) pattern (Fig. S8†).

The composition of the soaked electrode surface was analyzed by X-ray photoelectron spectroscopy (XPS). As observed in the N 1s spectrum (Fig. 2h), C–N and $–NH_2$ components were detected on the Zn negative electrode after Cy-H immersion, which were absent after immersion in ZSO. S 2p spectra (Fig. S9a and b†) showed that SO_4^{2-} components were detected at the SO_4^{2-} immersed Zn anode, which was attributed to the by-products.[40] In contrast, no component signal of SO_4^{2-} was detected at the Zn anode after Cy-H immersion, but a small amount of signal attributed to –SH was detected at 163.24 eV (Fig. S9a†), which confirms the adsorption behavior of Cy. Although Cy-H can be adsorbed on the surface of the electrode to avoid its corrosion under static conditions, it is still unknown whether Cy-H can protect the electrode from strong acid attack in the presence of an applied electric field.[13] For this reason, the conjecture will be verified by two classical tests, linear sweep voltammetry (LSV) and Tafel curves, where the results of the LSV test (Fig. 2i) show that Cy-H has the highest onset potential (−1.15 V), ZSO has an onset potential of −1.11 V, and the electrolyte with added HCl shows the worst result for the onset potential (−1.08 V).[41] Similarly, in the Tafel test results (Fig. 2j), Cy-H has the best performance in terms of corrosion potential (−0.969 V) and corrosion current (0.05 mA cm^{-2}), and ZSO (−0.974 V, 0.1 mA cm^{-2}) still performs better than HCl (−0.98 V, 0.5 mA cm^{-2}). The results show that only the addition of HCl aggravates the HER and electrochemical corrosion of the electrode, whereas the addition of Cy-H enables the electrode to show superior corrosion resistance and HER inhibition in ZSO in a strongly acidic environment.[42] This indicates that Cy-H can be effectively adsorbed on the surface of the electrode against the influence of strong acid solutions, endowing the electrode with the ability to carry out electrochemical reactions in acidic solutions without receiving erosion, a previously unreported and miraculous property.[43]

The optimal additive concentration needs to be determined before Zn symmetric cell tests, so we tested 0.005 M, 0.01 M, 0.015 M, 0.02 M, and 0.03 M at a current density of 5 mA cm^{-2} and a fixed capacity of 1 mA h cm^{-2}. As shown in Fig. S10, Cy-H† with 0.01 M possesses a cycle life of more than 750 h, whereas the cycle life of the symmetric cell starts to shrink drastically when the additive concentration exceeds 0.01 M. Therefore, 0.01 M was chosen as the optimal concentration to be used in subsequent research.[44] Under cycling conditions of 1 mA cm^{-2} and 0.5 mA h cm^{-2} (Fig. 3a), Cy-H exhibited an exceptionally long cycle life of 3000 h, while pure ZSO showed an unexpected short circuit after 100 h of cycling. As a comparison, the symmetric cell with added HCl (0.01 M) also exhibited a cycle life of less than 200 h. This result demonstrates that the addition of HCl does not improve the cycling performance of the symmetric cell, and through the addition of Cy-H can the cycle life of the Zn anode be significantly extended, which is attributed to the adsorptive protective effect of Cy-H, avoiding the corrosive behavior of HCl on the electrode and the generation of by-products.[45] Fig. 3b shows the operation of the Zn||Zn symmetric cell at 1 mA cm^{-2}, 1 mA h cm^{-2}. Cy-H still demonstrates a perfect cycling result of 2600 h, while both HCl and ZSO fail in less than 150 h.[46] Meanwhile, Cy-H showed the maximum polarization voltage in the cycle (Fig. S11†), followed by HCl, and ZSO showed the minimum polarization voltage, which may be due to the introduction of additives increasing the resistance to Zn deposition.[47] Furthermore, the voltage profile of the symmetric cell reveals comparable results in the case of 1 mA cm^{-2} and 1 mA h cm^{-2}, and Cy-H continues to have the maximum polarization voltage (Fig. S12†). Concurrently, the SEM images after cycling with Cy-H, HCl, and ZSO

are depicted in Fig. S13–S15,† and there are no by-products and glass fiber attachment on the surface after Cy-H cycling, although the surface after HCl cycling was flatter and free of by-products, but some of the Zn deposits showed incompleteness, probably due to strong acid corrosion, and finally the surface after ZSO cycling showed by-product formation and glass fiber attachment.[48] The addition of Cy-H and HCl can effectively eradicate the generation of by-products and promote the flat deposition of Zn, while ZSO will promote the attachment of by-products on the surface of the Zn anode and aggravate the growth of Zn dendrites.[49]

Furthermore, HCl was thought to be somehow associated with the elimination of by-products, but the addition of HCl alone was not feasible, so an interesting cycling procedure was devised: the Zn symmetric cell was first assembled using ZSO as the electrolyte and then left stationary for 24 h after depositing/stripping it 5 times at 1 mA cm^{-2} and 0.5 mA h cm^{-2}, followed by depositing/stripping 5 cycles, finally leaving it stationary for 24 h.[50] This process ensures a massive generation of by-products, yielding a Zn anode with a large number of dendrites and by-products, and the disassembled symmetric cell is shown in the digital photograph in Fig. 3c. Subsequently, the Zn anode with by-products was detached and matched with a new separator and counter electrode, and a new Zn symmetric cell was reassembled by adding Cy-H electrolyte and recycled under cycling conditions of 1 mA cm^{-2} and 0.5 mA h cm^{-2}. Impressively, such a symmetric cell was cycled for more than 2000 h, and the disassembled electrodes after cycling showed less glass fiber attachment and by-product generation than before.[51] On the other hand, the symmetric cell still using the ZSO with a new diaphragm and counter electrode failed after only less than 100 h of cycling (Fig. 3d), and the disassembled Zn anode electrode after cycling has more glass fibers and gray by-products adhered to it. This reinforces the fact that the addition of Cy-H was effective in reducing byproducts and was able to cycle a stable symmetric cell despite the presence of large amounts of byproducts at the electrodes and was able to eliminate some of the byproducts that had been generated, which has not been previously reported and which will be explained in a detailed investigation subsequently.[52] Next, the rate performance of the Zn||Zn symmetric cell was investigated using different electrolytes at current densities from 1 mA cm^{-2}

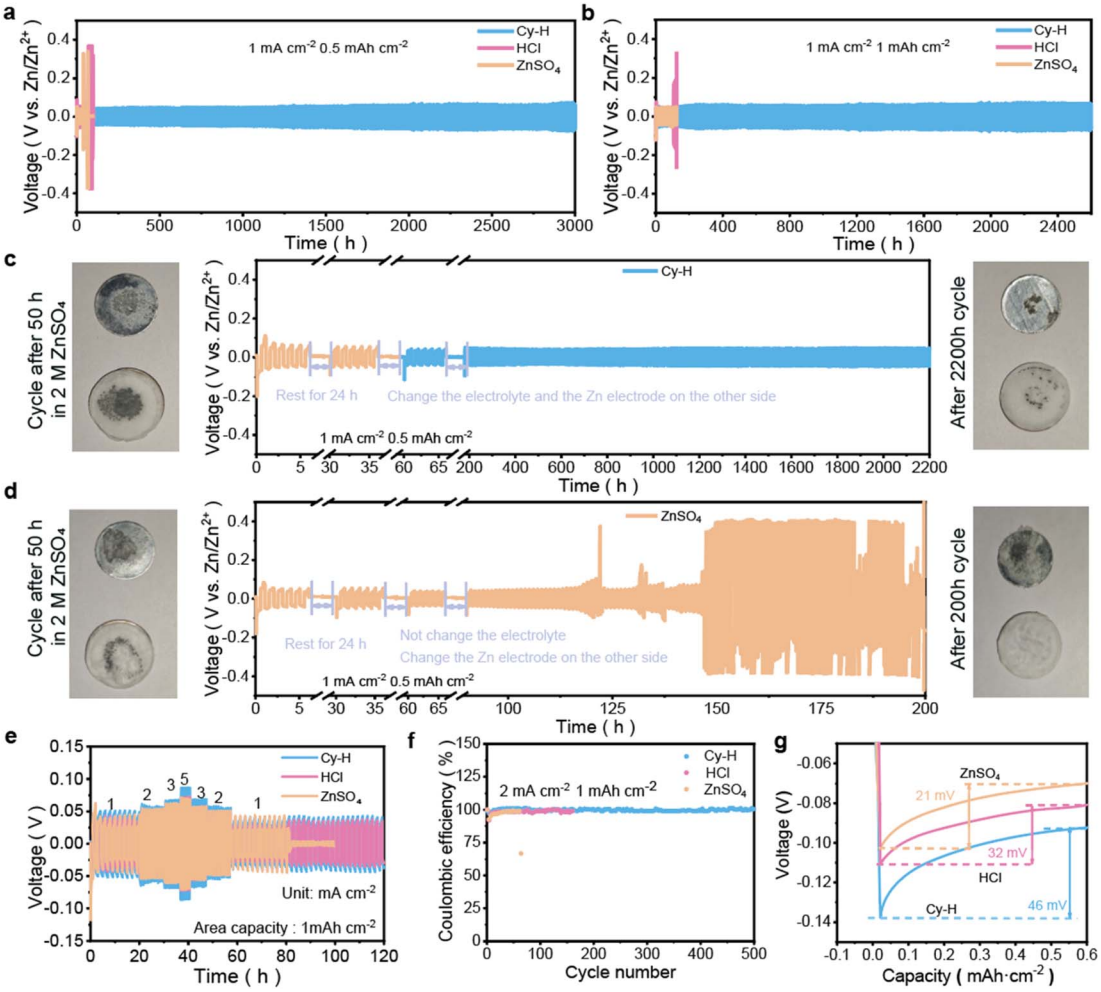

Fig. 3 Voltage profiles of Zn||Zn symmetric cells at (a) 0.5 and (b) 1 mA h cm^{-2}; voltage profiles of Zn||Zn symmetric cells with Cy-H (c) and ZSO (d) for by-product elimination; (e) rate performance of Zn||Zn cells at different current densities; (f) CE of Cu||Zn asymmetric cells using different electrolytes; (g) nucleation overpotential of the first cycle of Zn||Cu asymmetric cells in different electrolytes.

to 5 mA cm^{-2} (Fig. 3e). Cy-H exhibits excellent performance and stable voltage polarization throughout the cycling process. Fig. 3f shows the cycling performance of different electrolytes in Zn||Cu asymmetric cells, where Cy-H exhibits 500 stable cycles, while HCl and ZSO show fluctuations in coulombic efficiency at 180 and 90 cycles, respectively, followed by failure. Meanwhile, Cy-H exhibits a nucleation overpotential (Fig. 3g) of 46 mV, which exceeds that of HCl (32 mV) and ZSO (21 mV). This suggests that the addition of Cy-H and HCl favors the uniform nucleation of zinc by increasing the Zn nucleation energy barrier.

In order to investigate the protection mechanism of Cy-H on the Zn anode, MD simulations were carried out to observe the distribution of the components in Cy-H and ZSO. As shown in Fig. S16a,† after the addition of Cy-H, the number density of Zn^{2+} was almost twice as high as that of the original (in ZSO), and the distribution distance was 5 nm according to the electrode, which is about the thickness of the inner Helmholtz plane (IHP), suggesting that the addition of additives promotes the aggregation of Zn^{2+} at the boundaries of the IHP.[53] The distribution of water (Fig. S16b†) was also statistically obtained, which was significantly reduced in the IHP after the addition of Cy-H. This may be attributed to the fact that the additive molecules occupied the adsorption sites of the inner water, which caused the water molecules in the EDL to be excluded from the bulk phase and reduced the probability of the occurrence of side reactions.[54] To verify the results of the simulations, DEMS tests were carried out for different electrolytes to monitor *in situ* hydrogen emission during cell cycling. During the deposition/stripping of a Zn symmetric cell with Cy-H electrolyte, the device detected a periodic hydrogen precipitation behavior (Fig. 4a) that continued to diminish during the 6000 s cycling process, showing an outstanding HER suppression effect, which is consistent with the results hypothesized by the MD. In ZSO (Fig. S17†), the symmetric cell showed a strong HER behavior with a signal intensity nearly 1.5 times that of Cy-H, and the HER behavior was gradually intensified during the

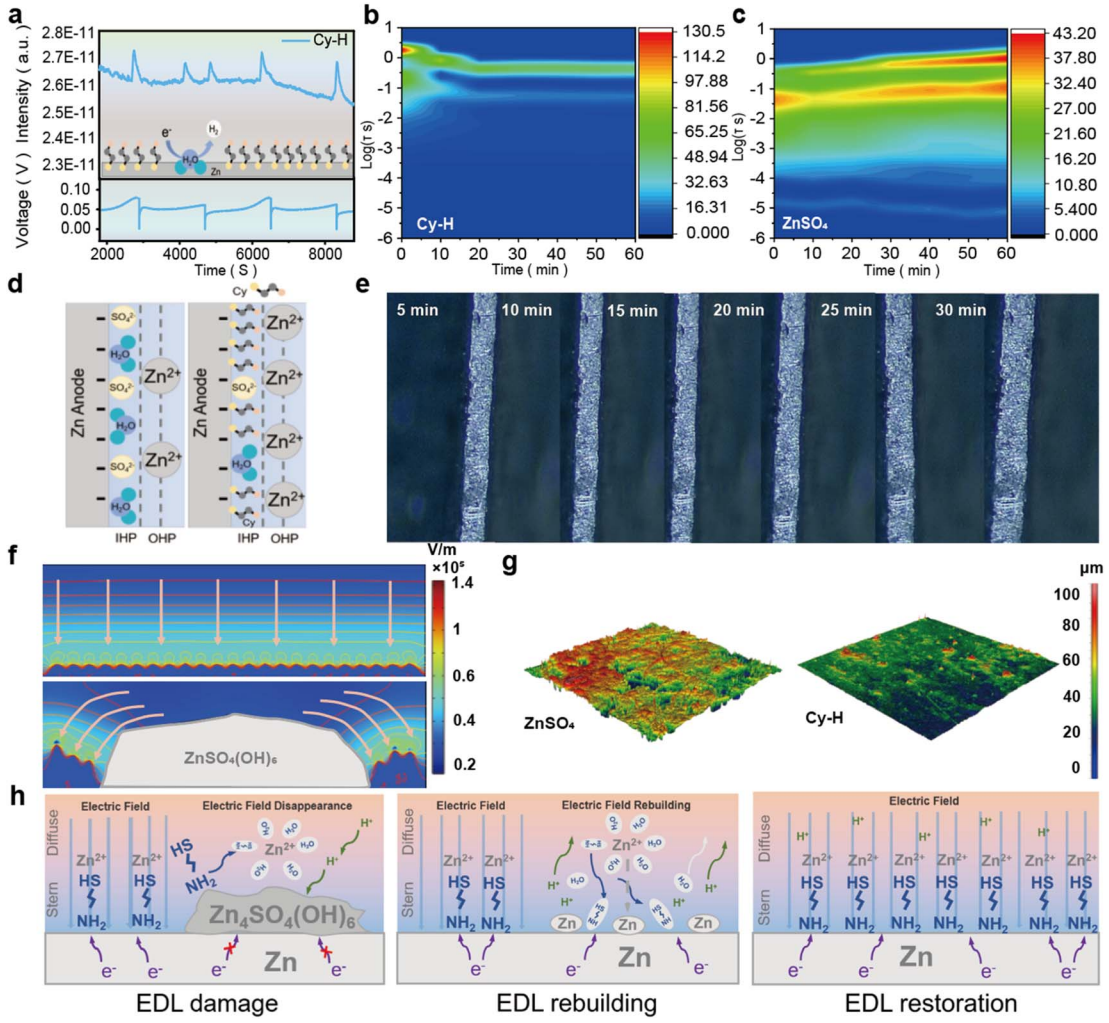

Fig. 4 (a) DEMS test pattern of Cy-H; *in situ* DRT spectra of Cy-H (b) and ZSO (c); (d) structure of EDLs with different electrolytes; (e) *in situ* optical images of the Zn plating on the Zn anode in Cy-H; (f) distribution of Zn^{2+} concentration on different electrode surfaces; (g) optical 3D surface profiler image of different electrolytes; (h) a schematic illustration of the Cy-H-specific immunological mechanism for safeguarding the Zn anode.

cycling process, which indicated the rampant occurrence of side reactions.[55]

In EDL theory, the aggregation of more cations at the IPH then implies that the EDL capacitance of the electrode will be enhanced.[56] Therefore, the EDL capacitance was tested by electrochemical impedance spectroscopy (EIS) equivalent circuit fitting and the CV method, and the results are shown in Fig. S18 and S19.† The results show that the capacitance of the EDL is significantly enhanced after the addition of Cy-H by either test method, indicating that the introduction of Cy-H causes the original EDL structure to change. The addition of HCl does not affect the capacitance of the EDL, which excludes the possibility that HCl changes the EDL at the electrode interface. In the solid–liquid interface of the battery, the EDL assumes an important role in ion transport, and the kinetic characteristics of the transport process will be determined by its structure and properties when the external load is applied to break the homeostasis of each component of the battery, where the difference in the relaxation caused by the current induced response of each component can correspond to a specific time constant, and therefore the distribution of relaxation times (DRT) technique has been adopted to investigate the behavior of Zn deposition in different electrolyte systems for a more detailed and scientific interpretation of the deposition results.[57]

The initial EIS was first tested using Cy-H and ZSO assembled into different symmetric cells, followed by EIS measurements every 10 min of deposition at a current of 1 mA cm^{-2}, and the results are shown in Fig. S20.† Subsequently, the EIS was converted into a DRT plot for analysis, and in Fig. S21,† it can be seen that a total of two characteristic peaks appeared in Cy-H, which can be attributed to the desolvation energy barriers of Zn^{2+} in the IPH and the hindering behaviors when they pass through the adsorbed Cy in the inner layer of the IPH, whereas three characteristic peaks were observed in ZSO, which also corresponded to the desolvation of hydrated Zn^{2+}, and the remaining two are attributed to the hindering behavior of SO_4^{2-} and H_2O, with water molecules being released earlier (and more frequently) than SO_4^{2-} due to their polarity and closer proximity to the electrode surface. It is worth noting that the adsorption of additives increases the hindrance during ion transport, so the intensity of all the characteristic peaks of Cy-H is greater than that of ZSO, which also corresponds to the polarization voltage of the previous symmetric cell. After confirming the meaning of the characteristic peaks of different electrolytes in DRT, all the EIS plots were transformed to DRT, and the results are shown in Fig. 4b, c, and S22.† In the symmetric cell using Cy-H electrolyte, the characteristic peaks of Zn^{2+} desolvation and the characteristic peaks caused by additive hindrance gradually weakened and shifted to a higher frequency during the deposition process, which indicates that the deposition process of Zn^{2+} tends to be easier and the structure of the EDL becomes gradually compact, maintaining a stable and strong interfacial region. In ZSO, the characteristic peaks of Zn^{2+} desolvation and the characteristic peaks generated by the obstruction of the other two ions all showed the behavior of decreasing and then increasing, and with the prolongation of the deposition time, these characteristic peaks were shifted to lower frequencies, which verified that the structure of the EDL was dynamic and tended to loosen gradually during the deposition process and that such behavior was not conducive to the deposition of Zn^{2+} and the stability of the electrochemical reaction. Therefore, we can confirm that the bilayer structure at the electrode interface before and after the addition of Cy-H is shown in Fig. 4d, and the addition of the additive will reduce the adsorption sites of H_2O and SO_4^{2-} in the IPH and increase the adsorption behaviors of cations on the boundary of the IHP, and the stabilized EDL composed of Cy-H is also conducive to the homogeneous deposition of Zn^{2+}.

An *in situ* optical microscope was employed as the most direct means of detecting the growth of dendrites to observe the deposition behavior of Zn^{2+} in different electrolytes. For the Zn anode in Cy-H, a smooth and homogeneous surface was observed throughout the Zn deposition process, whereas for the Zn anode in ZSO (Fig. S23†), dendrites were gradually produced and grew rapidly during the deposition process, accompanied by the HER. In the process of metal deposition, an acidic plating solution tends to refine the size of deposited grains and inhibit the growth of dendrites, so HCl was also used as a comparison for the observation of dendrite growth. The Zn anode also showed a smooth surface during the growth process, and no dendrites were observed, but the HER occurred due to the strong acidity of the electrolyte, which indicates that the introduction of HCl can improve the deposition behavior of Zn but increases the probability of HER generation (Fig. S24†). The process of dendrite growth is often accompanied by the generation of by-products, but most studies focus on the distribution of the electric field and the influence of the concentration distribution of zinc ions on the growth of Zn dendrites and do not pay attention to the interconnection between by-products and dendrites.

Through finite element simulation, we believe that the generation of by-products also promotes the growth of Zn dendrites, which are modeled as shown in Fig. S25a and b.† At the initial stage of model growth, the Zn anode without by-products was set with a row of uniform Zn growth sites, and on the surface of the Zn anode with by-products, three growth sites were set on the left and right sides, and the non-conducting by-products covered the growth sites in the middle. When the growth time reached 60 s, the results of dendrite growth are shown in Fig. S25c and d.† The Zn anode without by-products achieved uniform Zn deposition without the HER, while the Zn anode with by-products experienced accelerated Zn dendrite growth. When the time was extended to 90 s, the results are shown in Fig. S25e and f.† The smooth Zn anode still showed uniform deposition of Zn, while the Zn anode with by-products showed more rampant Zn dendrite growth. In order to analyze the reason, the concentration fields of the model were counted (Fig. S26a and b†), which showed that the distribution of Zn concentration was uniform on the smooth Zn anode surface, whereas when there was a by-product adhering to the Zn anode surface, the Zn^{2+} ions that were not consumed in the vicinity of the by-products would diffuse rapidly down the concentration gradient to the left and right ends of the Zn dendritic growth sites, which resulted in more Zn^{2+} ions being available to the remaining growth sites,

accelerating the rampant growth of dendrites. Meanwhile, the electric field distribution during the growth process is also shown in Fig. 4f. The electric field distribution of the smooth zinc anode tends to be homogeneous. In contrast, the surface of the Zn anode to which the byproducts are attached will form distorted electric field lines, which will accelerate the diffusion of Zn^{2+} from other regions to the Zn deposition sites, and the deposition sites that have received more Zn^{2+} will gradually evolve into coarse dendrites to disrupt the cycle of the cell. Similarly, similar results have been observed using an optical 3D surface profiler (Fig. 4g), where the surface attachment of glass fibers/by-products (non-sharp areas in the image are defined as by-products attachment) is always accompanied by the growth of a large number of dendrites, whereas on the surface of the electrodes that are almost free of by-products and glass fibers, there are only sparse dendrites of small sizes.

Therefore, a schematic illustration of the Cy-H specific immunological mechanism for safeguarding the Zn anode was proposed (Fig. 4h): when the Zn anode is immersed in the electrolyte, Cy starts to actively seize the sites of H_2O and SO_4^{2-} in the IHP (stern layer), and Cy adsorbed on the electrode surface makes a large amount of Zn^{2+} line up on the outer side of the IPH, prevents H^+ from approaching the electrode due to the charge effect. Subsequently when the by-products are generated, the insulating properties of the by-products weaken the electric field at Zn anode, makes it difficult to continue the initial structure of the EDL, allowing the Cy molecules to resolve and participate in solventization structure of Zn^{2+} in solution, and Zn^{2+} is no longer no longer bound to the IPH edge, at which time the H^+ gradually corrodes the $Zn_4(OH)_6SO_4 \cdot xH_2O$ through spontaneous acid–base neutralization reactions and regenerates the Zn^{2+} and H_2O, when the by-products are eliminated, the re-establishment of the electric field makes the EDL structure reconstituted on the surface of Zn anode, and during Zn deposition process, Zn^{2+} will carry Cy molecules adsorbed on the surface of the electrode (in the theory of EDL no cations can be present in the IPH, so H^+ is excluded from the IPH boundary layer), and the adsorption of Cy begins to make the Zn^{2+} (the divalent cations Zn^{2+} is subjected to stronger electric field forces than the monovalent cation H^+) to accumulate at the IPH edge thereby crowding out H^+, the effect of corrosion by H^+ is rejected. Through this synergistic effect, the electrolyte's "specific" elimination of by-products from the Zn anode is realized.[58]

To verify the suitability of the electrolyte additives, we assembled Zn||I_2 full cells using Cy-H, HCl, and ZSO electrolytes. The full-cell CV curves in different electrolytes are shown in Fig. 5a. They exhibit similar shapes and all the electrolytes can keep the shape of the CV curves stable at different sweep speeds (Fig. S27a–c†), which suggests that the addition of additives does not interfere with the electrochemical reactions of the full cell. The initial EIS of the full cell was subsequently measured (Fig. S28†) with the addition of Cy-H and HCl, showing lower charge transfer resistance (R_{ct}) and larger diffusion rates relative to ZSO, which could be attributed to the acidic environment accelerating the ion transport process. In the subsequent rate test (Fig. 5b), Cy-H showed excellent

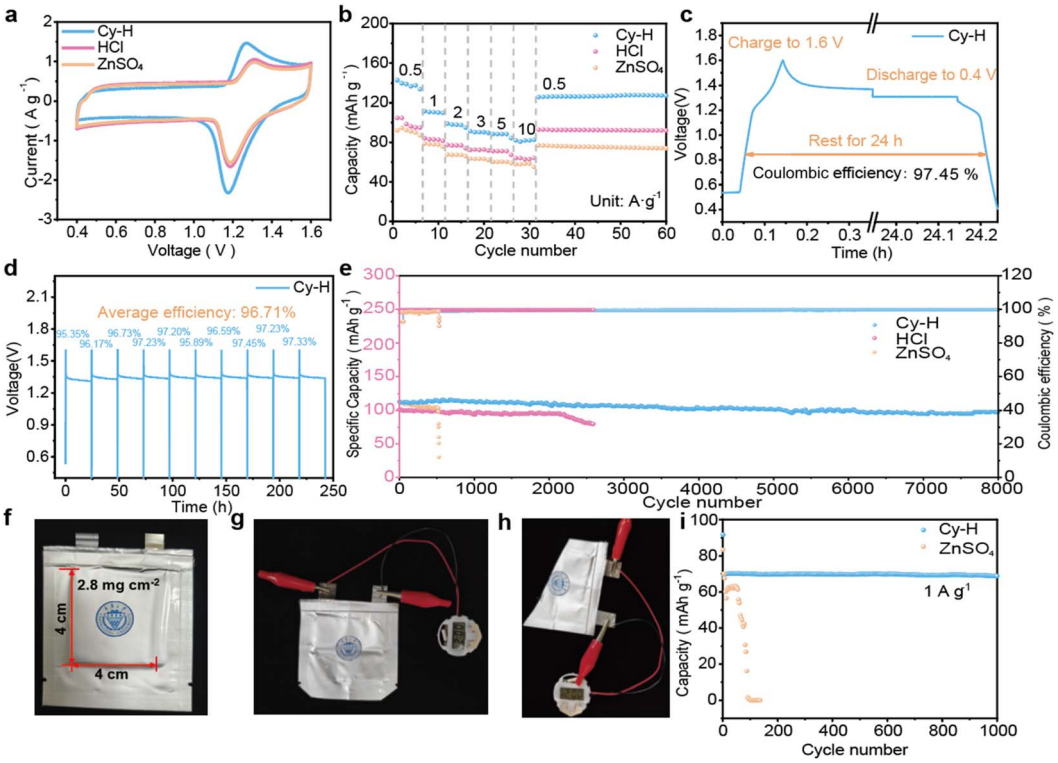

Fig. 5 CV curves (a) and rate performance (b) of Zn//I_2 full cells with different electrolytes; self-discharge (c) and ten consecutive self-discharge tests (d); (e) long-term cycling performance of the Zn//I_2 full cells at 2 A g^{-1}. Digital photograph of a pouch battery (f) and it powering a watch under normal (g) and flexed (h) conditions. (i) Long-term cycle performance at 1 A g^{-1} of assembled pouch batteries with different electrolytes.

performance and the shape of the curve was well preserved with increasing current density, as can be seen in the charge/discharge curves (Fig. S29a–c†) compared to HCl and ZSO. Self-discharge of aqueous batteries is also one of the challenges that limit their practical application, so different electrolytes were tested for self-discharge, and in the full battery with Cy-H electrolyte, the battery still exhibited a capacity retention of 97.45% after 24 h of rest (Fig. 5c) and showed an average of 96.71% capacity retention in 10 subsequent consecutive self-discharge tests (Fig. 5d), which is an impressive result. In Fig. S30,† HCl also demonstrated more excellent self-discharge retention (96.38%, average retention 93.67%), while ZSO only showed 85.55% highest capacity retention and 81.59% average capacity retention (Fig. S31†). Finally, during the long-term cycling of the full cell, Cy-H demonstrated ultra-long cycling performance of 8000 cycles and 95% capacity retention, while HCl and ZSO only showed cycling performance of 2000 and 500 cycles (Fig. 5e). In the post-cycling EIS image (Fig. S32†), Cy-H and HCl still maintain a low impedance, while the impedance of ZSO increases dramatically, which may be caused by the accumulation of by-products. In order to verify the practicality of the present strategy, a pouch battery with a cathode loading of 2.8 mg cm^{-2} was assembled, with the shape shown in Fig. 5f. Under normal conditions, it can effectively power an electronic watch and a small light bulb (Fig. 5g and S33†), and it can provide energy output normally even under extreme conditions such as bending and shearing (Fig. 5h and S34†). Surprisingly, at a current density of 1 A g^{-1}, the assembled pouch battery achieved 1000 cycles without degradation, whereas the battery assembled with the ZSO electrolyte failed after 100 cycles, which proves the significant effect of the Cy-H additive on the stability of the Zn anode interface (Fig. 5i).

For analyzing the inhibition mechanism of Cy-H on the prominent self-discharge of the full cell, the DRT technique will be employed to analyze the dominant factors of self-discharge. First, the initial DRT images of the symmetric cell with I_2 and Zn and the Zn||I_2 full cell are shown in Fig. 6a and b. In the symmetric cell with I_2, Cy-H exhibits two peaks at 0–0.01 Hz, which are attributed to the aggregation of I_3^- and H^+ caused by the electrode interface, and shows larger diffusion hindrance in the low-frequency region, which is favorable for inhibiting the free diffusion of H^+. The image of the Zn symmetric cell is similar to the previous analysis. Finally, when the DRT image of the assembled Zn||I_2 full cell in the fully charged state is shown in Fig. 6c, it can be seen that the main characteristic peaks are still located in the low-frequency region induced by the diffusion behavior, and the ZSO shows a stronger diffusion behaviour. The second outgoing peak at 0.01 Hz can be attributed to the peaks caused by the formation of EDL after Zn deposition at the interface of the anode, and the reason why the intensity of the characteristic peaks of Cy-H is lower than that of ZSO is due to the formation of a more stable EDL structure.[59]

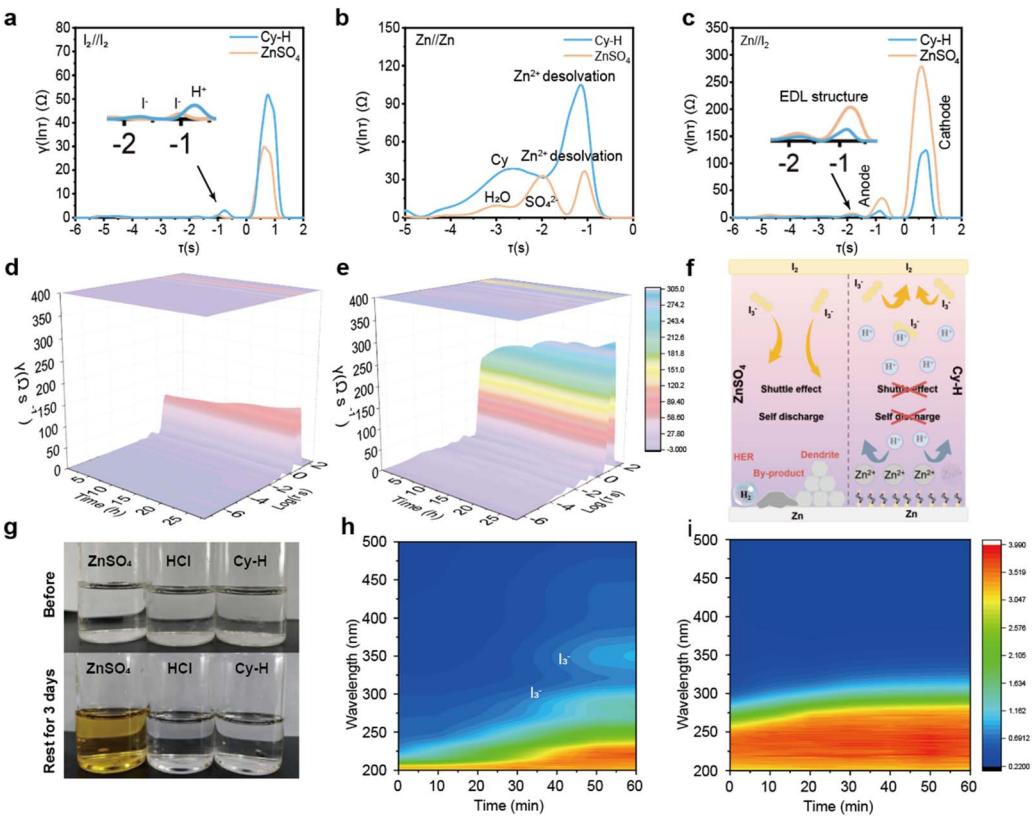

Fig. 6 DRT spectra of I_2//I_2 (a), Zn//Zn (b) and Zn//I_2 (c) with different electrolytes; *in situ* DRT spectra during self-discharge of Cy-H (d) and ZSO (e); schematic diagram of the self-discharge suppression mechanism (f); (g) immersion experiment in different electrolytes; *in situ* surface UV of ZSO (h) and Cy-H (i).

Subsequently, the DRT profiles were collected every 4 h during a 28 h long self-discharge process, and the results are shown in Fig. 6d, e and S35.† The full cell with Cy-H electrolyte shows a gradual but slower increase in diffusion behavior in the low-frequency region and a weak enhancement of the characteristic peaks at 0.01 Hz, which corresponds to the thermodynamically driven relaxation of the EDL structure at the anode, but not significant, and the gradual increase of small characteristic peaks in the high-frequency region is worth noting, which is caused by the generation of by-products on the surface of the Zn anode. The whole cell with ZSO electrolyte shows a sharp increase of diffusion in the low-frequency region during the whole self-discharge process, and the characteristic peaks at 0.01 Hz also show more obvious signs of enhancement. Therefore, the self-discharge process of the full cell is shown in Fig. 6f, in ZSO electrolyte, the I_3^- of the positive electrode undergoes obvious diffusion behavior, and the Zn anode electrode also produces various side reactions such as by-product generation and the HER during the deposition process, which results in serious self-discharge. As for the full battery with Cy-H electrolyte, I_3^- at the cathode was inhibited from freely diffusion in the acidic environment, avoiding shuttling by I_3^-, and the stable EDL structure on the surface of the Zn anode and the specific immune mechanism of HCl made it possible to eliminate the accumulation and attachment of the by-products, thus showing superior self-discharge inhibition performance. To demonstrate the inhibition mechanism of H^+ for I_3^-, 1 mg of iodine was submerged in three different sets of electrolytes. After three days, the ZSO electrolyte showed significant discoloration, which confirmed the rapid diffusion of I_3^-, while no significant discoloration behavior was observed in the HCl and Cy-H electrolytes (Fig. 6g). Finally, the UV signals of the electrolyte during the constant-current discharge of the cell were detected *in situ* by our own fabricated *in situ* UV observation device (Fig. S36†). The results, as shown in Fig. 6h and i, show that the enhancement of the signal of I_3^-, which is caused by the free diffusion of I_3^-, gradually appeared near 280 nm and 350 nm during the discharge of the full cell using ZSO electrolyte. In the full cell assembled with Cy-H electrolyte, on the other hand, the appearance of new characteristic peaks was not found, which indicated that Cy-H effectively suppressed the shuttling effect of I_3^-.

Conclusion

In this work, an innovative strategy for targeted elimination of by-products at the Zn anode interface was developed by the introduction of Cy-H. The spontaneous adsorption of Cy-H optimizes the EDL structure at the Zn anode interface, which protects the Zn anode from HCl corrosion and effectively inhibits the HER behavior in the electrochemical reaction by expelling H_2O and SO_4^{2-}. The introduction of an acidic environment also achieves the targeted elimination of by-products at the interface, which avoids the potential danger of the rampant growth of dendrites and the accumulation of by-products. Ultimately, in the assembled Zn‖I_2 full cell, an ultra-long cycle of 8000 cycles was achieved and the assembled pouch battery also achieved 1000 cycles without capacity degradation. The self-discharge behavior of the full cell was effectively improved, and the effect of Cy-H on the cathode was also explored. Therefore, this work on electrolyte additives will strongly advance the work on by-product elimination, and its excellent low self-discharge performance also shows great potential for application.

Data availability

The authors confirm that the data supporting the findings of this study are available within the article and its ESI.†

Author contributions

Kaixin Wang: conceptualization, data curation, and investigation. Yuting He: data curation. Ruduan Yuan: data curation. Zhaoyu Chen: resources. Qianzhi Gou: data curation. Sida Zhang: writing – original draft. Huaping Mei: writing – original draft. Yujie Zheng: writing – original draft. John Wang: resources. Meng Li: resources and funding acquisition.

Conflicts of interest

The authors declare no conflicts of interest.

Acknowledgements

This work was financially supported by research grants from the Natural Science Foundation of China (52173235), the Hainan Province Science and Technology Special Fund (ZDYF2024SHFZ038), the National Key Research and Development Program of China (2022YFB3803300), and the Venture & Innovation Support Program for Chongqing Overseas Returnees (CX2021018). We would like to thank the Analytical and Testing Center of Chongqing University for their support in materials characterization.

References

1 Z. Jiao, X. Cai, X. Wang, Y. Li, Z. Bie and W. Song, *Adv. Energy Mater.*, 2023, **13**, 2302676.
2 Y. Dai, C. Zhang, J. Li, X. Gao, P. Hu, C. Ye, H. He, J. Zhu, W. Zhang, R. Chen, W. Zong, F. Guo, I. P. Parkin, D. J. L. Brett, P. R. Shearing, L. Mai and G. He, *Adv. Mater.*, 2024, **36**, 2310645.
3 Y. Mu, Y. Chen, B. Wu, Q. Zhang, M. Lin and L. Zeng, *Adv. Sci.*, 2022, **9**, 2203321.
4 M. Zhu, H. Wang, H. Wang, C. Li, D. Chen, K. Wang, Z. Bai, S. Chen, Y. Zhang and Y. Tang, *Angew. Chem., Int. Ed.*, 2024, **63**, 202316904.
5 H. Li, S. Li, R. Hou, Y. Rao, S. Guo, Z. Chang and H. Zhou, *Chem. Soc. Rev.*, 2024, **53**, 7742.
6 Q. Huang, Y. Gao, J. Sun, B. Liu, X. Liu, Y. Pang, Y. Liu and J. Wang, *DeCarbon*, 2024, **4**, 100049.

7 B. D. Boruah, A. Mathieson, B. Wen, S. Feldmann, W. M. Dose and M. De Volder, *Energy Environ. Sci.*, 2020, **13**, 2414.
8 Y. Zhao, P. Zhang, Y. Qiu, Q. Li, H. Yan, Z. Wang and C. Wu, *DeCarbon*, 2024, **5**, 100051.
9 Q. Guo, G. Teri, W. Mo, J. Huang, F. Liu, M. Ye and D. Fu, *Energy Environ. Sci.*, 2024, **17**, 2888.
10 J. Sun, J. Zhang, S. Wang, P. Sun, J. Chen, Y. Du, S. Wang, I. Saadoune, Y. Wang and Y. Wei, *Energy Environ. Sci.*, 2024, **17**, 4304.
11 M. Liu, P. Wang, W. Zhang, H. He, G. He, S. Xu, L. Yao and T. S. Miller, *Energy Storage Mater.*, 2024, **67**, 103248.
12 Y. Yu, X. Jia, Q. Zhang, H. Song, P. Zhang, F. Wang and J. Liu, *J. Colloid Interface Sci.*, 2024, **677**, 748.
13 X. Qian, T. Chen, Y. Wang, Q. Zhang, W. Li and J. Fu, *Angew. Chem., Int. Ed.*, 2024, **63**, 202412989.
14 D. Li, Y. Yu, W. Zhao, F. Wang, Y. Su and L. Cao, *Nano Energy*, 2024, **128**, 109806.
15 T. Krausgruber, N. Fortelny, V. Fife-Gernedl, M. Senekowitsch, L. C. Schuster, A. Lercher, A. Nemc, C. Schmidl, A. F. Rendeiro, A. Bergthaler and C. Bock, *Nature*, 2020, **583**, 296.
16 J. Zhang, C. Qiu, C. Zhou, S. Guo, Y. Gao, F. Li, X. Wang, Z. Zhao, Z. Xing, J. Li, P. Rao, Z. Kang, X. Tian and X. Shi, *Nano Energy*, 2025, **133**, 110519.
17 Q. Nian, X. Luo, D. Ruan, Y. Li, B.-Q. Xiong, Z. Cui, Z. Wang, Q. Dong, J. Fan, J. Jiang, J. Ma, Z. Ma, D. Wang and X. Ren, *Nat. Commun.*, 2024, **15**, 4303.
18 L. E. Blanc, D. Kundu and L. F. Nazar, *Joule*, 2020, **4**, 771.
19 L. Li, Y. Chen, S. Wang, D. Pei, M. Li, T. Li and C. Li, *Nano Energy*, 2024, **126**, 109662.
20 R. Li, H. Xiang, Q. Liang, Y. Zhou, X. Ma, D. Chao, M. Xin, H. Yuan and X. Jia, *Nano Energy*, 2024, **128**, 109946.
21 S. Zhang, Q. Gou, W. Chen, H. Luo, R. Yuan, K. Wang, K. Hu, Z. Wang, C. Wang, R. Liu, Z. Zhang, Y. Lei, Y. Zheng, L. Wang, F. Wan, B. Li and M. Li, *Adv. Sci.*, 2024, **11**, 2404968.
22 Q. Gou, Z. Chen, H. Luo, J. Deng, B. Zhang, N. Xu, J. Cui, Y. Zheng, M. Li and J. Li, *Small*, 2024, **20**, 2305902.
23 Y. Mu, M. Han, J. Li, J. Liang and J. Yu, *Carbon*, 2021, **173**, 477.
24 Y. Mu, Y. Chu, L. Pan, B. Wu, L. Zou, J. He, M. Han, T. Zhao and L. Zeng, *Int. J. Extreme Manuf.*, 2023, **5**, 042008.
25 Y. Hang, L. Li, C. Duo, W. Jingyi, T. Yicheng, J. Zhenjing, Z. Yiming, M. Chenglin, Z. Wei, H. Wei and H. Guanjie, *Angew. Chem., Int. Ed.*, 2025, **64**, 202419394.
26 Q. Gou, H. Luo, Q. Zhang, J. Deng, R. Zhao, O. Odunmbaku, L. Wang, L. Li, Y. Zheng, J. Li, D. Chao and M. Li, *Small*, 2023, **19**, 2207502.
27 J. He, Y. Mu, B. Wu, F. Wu, R. Liao, H. Li, T. Zhao and L. Zeng, *Energy Environ. Sci.*, 2024, **17**, 323.
28 H. Yang, D. Chen, Y. Tan, H. Xu, L. Li, Y. Zhang, C. Miao, G. Li and W. Han, *J. Energy Chem.*, 2023, **81**, 101.
29 Q. Gou, H. Luo, L. Qu, F. Yu, K. Wang, S. Zhang, Z. Luogu, B. Zhang, Y. Zheng, B. Song, J. Wang and M. Li, *J. Energy Chem.*, 2025, **101**, 191.
30 Q. Gou, H. Luo, Y. Zheng, Q. Zhang, C. Li, J. Wang, O. Odunmbaku, J. Zheng, J. Xue, K. Sun and M. Li, *Small*, 2022, **18**, 2201732.
31 H. Yang, D. Chen, R. Zhao, G. Li, H. Xu, L. Li, X. Liu, G. Li, D. Chao and W. Han, *Energy Environ. Sci.*, 2023, **16**, 2910.
32 H. Yang, W. Zhou, D. Chen, J. Liu, Z. Yuan, M. Lu, L. Shen, V. Shulga, W. Han and D. Chao, *Energy Environ. Sci.*, 2022, **15**, 1106.
33 K. Wang, X. Fan, S. Chen, J. Deng, L. Zhang, M. Jing, J. Li, L. Gou, D. Li and Y. Ma, *Small*, 2023, **19**, 2206287.
34 J. Li, Z. Guo, J. Wu, Z. Zheng, Z. Yu, F. She, L. Lai, H. Li, Y. Chen and L. Wei, *Adv. Energy Mater.*, 2023, **13**, 2301743.
35 Q. Zhao, K. Sun, X. Wang, Q. Wang and J. Wang, *DeCarbon*, 2024, **3**, 100034.
36 J. Wang, Y. Zhou, J. Li, L. Zhao, Y. Zhu, Y. Wang, R. Wu, Y. Wang, D. J. Blackwood and J. S. Chen, *DeCarbon*, 2024, **3**, 100037.
37 Z. Cai, J. Wang and Y. Sun, *eScience*, 2023, **3**, 100093.
38 J. E. Kenison, N. A. Stevens and F. J. Quintana, *Nat. Rev. Immunol.*, 2023, **24**, 338.
39 G. Oliveira and C. J. Wu, *Nat. Rev. Cancer*, 2023, **23**, 295.
40 A. Chen, Y. Zhang, Q. Li, G. Liang, S. Yang, Z. Huang, Q. Yang, H. Hu, X. Li, Z. Chen, J. Fan and C. Zhi, *Energy Environ. Sci.*, 2023, **16**, 4054.
41 J. Zhou, Y. Mei, F. Wu, Y. Hao, W. Ma, L. Li, M. Xie and R. Chen, *Angew. Chem., Int. Ed.*, 2023, **62**, 202304454.
42 Y. Zhu, G. Liang, X. Cui, X. Liu, H. Zhong, C. Zhi and Y. Yang, *Energy Environ. Sci.*, 2023, **17**, 369.
43 W. Ma, S. Wang, X. Wu, W. Liu, F. Yang, S. Liu, S. C. Jun, L. Dai, Z. He and Q. Zhang, *Energy Environ. Sci.*, 2024, **17**, 4819.
44 Y. Shang and D. Kundu, *Joule*, 2023, **7**, 244.
45 T. Xiao, J.-L. Yang, B. Zhang, J. Wu, J. Li, W. Mai and H. J. Fan, *Angew. Chem., Int. Ed.*, 2024, **63**, e202318470.
46 L. Tan, Y. Lin, Z. Zhong, G. Yang and C. Wang, *Chem. Eng. J.*, 2024, **502**, 157927.
47 X. Xie, X. Xu, S. Liang and G. Fang, *J. Energy Chem.*, 2025, **101**, 402.
48 X. Bai, Y. Nan, K. Yang, B. Deng, J. Shao, W. Hu and X. Pu, *Adv. Funct. Mater.*, 2023, **33**, 2307595.
49 K. Lu, H. Jing, Q. Guo, C. Liu, B. Liu, X. Xia, F. Wang, W. Lei, M. Xia and Q. Hao, *J. Energy Chem.*, 2025, **102**, 37.
50 Y. Wu, Y. Zhang, Y. Ma, J. D. Howe, H. Yang, P. Chen, S. Aluri and N. Liu, *Adv. Energy Mater.*, 2018, **8**, 1802470.
51 H. Meng, Q. Ran, T. Dai, J. Jia, J. Liu, H. Shi, G. Han, T. Wang, Z. Wen, X. Lang and Q. Jiang, *Adv. Mater.*, 2024, **36**, 2403803.
52 S. You, Q. Deng, Z. Wang, Y. Chu, Y. Xu, J. Lu and C. Yang, *Adv. Mater.*, 2024, **36**, 2402245.
53 J. Fu, Z. P. Cano, M. G. Park, A. Yu, M. Fowler and Z. Chen, *Adv. Mater.*, 2016, **29**, 1604685.
54 J. Shin, J. Lee, Y. Kim, Y. Park, M. Kim and J. W. Choi, *Adv. Energy Mater.*, 2021, **11**, 2100676.
55 Z. Yi, G. Chen, F. Hou, L. Wang and J. Liang, *Adv. Energy Mater.*, 2020, **11**, 2003065.

56 L. Hu, C. Dai, Y. Zhu, X. Hou, Z. Liu, X. Geng, H. Wang, J. Chen, N. Sun, Q. Rong, Y. Zhu, X. He and Y. Lin, *Energy Environ. Sci.*, 2024, **17**, 5552.
57 Q. Gou, S. Zhang, H. Mei, C. Liu, H. Luo, K. Wang, Y. Hu, B. Song, Y. Zheng, M. Qiao and M. Li, *J. Mater. Chem. A*, 2025, **13**, 7766.
58 S. Zhang, J. Chen, W. Chen, Y. Su, Q. Gou, R. Yuan, Z. Wang, K. Wang, W. Zhang, X. Hu, Z. Zhang, P. Wang, F. Wan, J. Liu, B. Li, Y. Wang, G. Zheng, M. Li and J. Sun, *Angew. Chem., Int. Ed.*, 2025, **64**, 202424184.
59 H. Luo, Q. Gou, Y. Zheng, K. Wang, R. Yuan, S. Zhang, W. Fang, Z. Luogu, Y. Hu, H. Mei, B. Song, K. Sun, J. Wang and M. Li, *ACS Nano*, 2025, **19**, 2427.